

Accurate X-Ray Absorption Predictions for Transition Metal Oxides: An Advanced Self-Consistent-Field Approach Inspired by Many-Body Perturbation Theory

Yufeng Liang,^{1,*} John Vinson,² Sri Pemmeraju,¹ Walter Drisdell,³ Eric Shirley,² and David Prendergast¹

¹*The Molecular Foundry, Lawrence Berkeley National Laboratory, Berkeley, CA 94720, USA*

²*National Institute of Standards and Technology (NIST), Gaithersburg, MD 20899, USA*

³*Chemical Sciences Division, Lawrence Berkeley National Laboratory, Berkeley, CA 94720, USA*

Constrained-occupancy self-consistent-field (Δ SCF) methods and many-body perturbation theories (MBPT) are two strategies for obtaining electronic excitations from first-principles. Using the two distinct approaches, we study the O 1s core excitations that have become increasingly important for characterizing transition metal oxides and developing theory of strong correlations. Interestingly, we find that the Δ SCF approach, in its current single-particle form, systematically underestimates the pre-edge intensity for chosen oxides, despite its success in weakly correlated systems. By contrast, the Bethe-Salpeter equation within MBPT predicts much better lineshapes. This inspires us to reexamine the many-electron dynamics of X-ray excitations. We find that the single-particle Δ SCF approach can be rectified by explicitly calculating many-body transition amplitudes, producing X-ray spectra in excellent agreement with experiments. Our study paves the way to accurately predict X-ray near-edge spectral fingerprints for physics and materials science beyond the Bethe-Salpeter equation.

X-ray absorption spectroscopy (XAS) is a powerful characterization technique to address challenging problems in physics, chemistry, and materials science, owing to its element specificity and orbital selectivity. With the help of density-functional theory (DFT), the interpretation of XAS is greatly facilitated by simulating spectral fingerprints for hypothetical structures from first-principles. Satisfactory X-ray absorption spectra have been simulated across a wide range of systems from small molecules [1, 2] to condensed-matter systems [3–9] and even complex interfaces [10].

Recently, interpreting XAS fingerprints for transition metal oxides (TMOs) from first-principles has become a pressing matter. In part, this is fueled by the quest for next-generation energy materials, for rechargeable battery cathodes [11–14], fuel cells [15, 16], water-splitting catalysts [17–19], and transparent conductive layers [20]. Many prototypes of these energy devices are TMOs with complex chemical properties due to their d orbitals. There is an enormous interest in how this electronic structure affects their functioning principles or failure mechanisms. Since the vast majority of these materials undergo inhomogeneous chemical reactions [11–13], and some of them exhibit complicated surface [15–18] and interfacial [19] behaviors, this makes X-ray spectroscopy particularly effective in revealing local chemical and structural properties.

Besides the immediate needs in materials research, understanding of the intriguing electron correlations inherent in TMOs can be advanced by the interpretation of core-level spectra. For instance, XAS has been employed to investigate the metal-insulator transitions induced by correlated effects [21–23], hole-doping-induced high- T_c superconductivity [24, 25], and, recently, emergent phenomena at perovskite interfaces [26]. Since core-level spectra reflect the energy distribution of orbitals of par-

ticular symmetries, they often serve as powerful guides to advance theories for correlated electron systems, including the DFT+U method [27], dynamical mean-field theory [28], and exact diagonalization approaches [29, 30].

Of particular interest in the study of TMOs is the O K edge that arises from the $1s \rightarrow 2p$ dipole-allowed transition. Since the O $2p$ orbitals can hybridize covalently with the metal d orbitals, the O K edge contains information on the d -state electronic structure that is crucial to many interesting phenomena in TMOs. Unlike the transition metal L -edge ($2p \rightarrow d$) spectra, O K edge spectra are not affected by core-level spin-orbit coupling and are free of atomic multiplet effects [31]. In almost all of the aforementioned examples [11, 13–15, 17–22, 24–27, 29, 30], there are measurements at the O K edge. Despite its utility, very few studies have simulated this absorption edge for TMOs from first-principles, limiting the interpretation of the spectra, because of the difficulty in treating both strong electron-electron ($e-e$) and electron-core-hole correlations adequately.

In this Letter, we present a first-principles study of the O K edge of TMOs, using two state-of-the-art theories of XAS simulation: (1) the constrained-occupancy self-consistent field (Δ SCF) core-hole approach [6, 7, 9] and (2) the core-level Bethe-Salpeter equation (BSE) within many-body perturbation theory (MBPT) [32–35]. Both theories yield absorbance $\sigma(\omega)$ with approximations to the many-body final state $|\Phi_f\rangle$ in Fermi's Golden rule,

$$\sigma(\omega) \propto \omega \sum_f |\langle \Phi_f | \epsilon \cdot \mathbf{R} | \Phi_i \rangle|^2 \delta(E_f - E_i - \hbar\omega) \quad (1)$$

where ϵ and \mathbf{R} are the photon polarization and many-body position operator respectively, and $|\Phi_i\rangle$ is the initial state. But the two theories differ in the underlying philosophy of solving the many-electron problem. As a Δ SCF method, the core-hole approach iterates the total elec-

tron density self-consistently with e - e interactions, while the BSE considers elementary excitations and treats e - e interactions perturbatively. One would expect a self-consistent theory works better than a perturbation theory. We find, however, that the one-body core-hole approach fails to describe the pre-edge region of the O K edge for TMOs, despite its success in producing XAS for many weakly correlated systems [9, 10, 36–38]. On the other hand, we show that the BSE is much more reliable for predicting XAS fingerprints for TMOs. The success of the BSE inspires us to examine both theories in a more general formalism, and ultimately demonstrate that the failure of the current Δ SCF approach can be rectified through proper evaluation of the many-body matrix elements.

Five TMOs are selected for benchmarking the first-principles XAS theories: the rutile phase of TiO_2 , VO_2 , and CrO_2 as well as the the corundum $\alpha\text{-Fe}_2\text{O}_3$ and the perovskite SrTiO_3 . They vary greatly in structure, band gap, or magnetism. The rutile VO_2 ($> 340\text{K}$) and CrO_2 are metallic, whereas TiO_2 and SrTiO_3 is insulating. CrO_2 is ferromagnetic (FM) while Fe_2O_3 is anti-ferromagnetic (AFM). The rest exhibit no magnetism. The O K edges from previous experiments [17, 21, 39–41] are shown in Fig. 1 (a). These spectra are angularly averaged except for CrO_2 , where the polarization is perpendicular to the magnetization axis [40]. The TM- $3d$ -O- $2p$ hybridization manifests as sharp double peaks around 530 eV, which result from the t_{2g} - e_g splitting in the octahedral field. The intensity ratio of the two peaks is sensitive to changes in hybridization or charge transfer and often serves as a diagnostic tool.

Core-Hole Approach The core-excited atom is treated as a single impurity with one electron removed from the excited core level. Depending on whether or not the X-ray photoelectron is added, the Δ SCF core-hole approach is termed as an excited-electron and core-hole (XCH) or full core-hole (FCH) calculation [6, 7, 9]. One then places the excited atom in a sufficiently large supercell to reduce spurious interactions between periodic replicas. The constrained-occupancy electron density is found using DFT. This modified ground state, including the presence of a core hole, is referred to as the *final state* [34], and that of the pristine system as the *initial state*. The working approximation is to map the many-electron system onto a set of Kohn-Sham orbitals

$$\langle \Phi_f | \epsilon \cdot \mathbf{R} | \Phi_i \rangle \approx S \langle \tilde{\phi}_f | \epsilon \cdot \mathbf{r} | \phi_h \rangle \quad (2)$$

where $\tilde{\phi}_f$'s are the unoccupied orbitals in the final state (with tilde) and ϕ_h is the core orbital in the initial state. S is the many-body overlap and is usually treated as a constant independent of excitation energy.

To account for strong electron correlations in TMOs, the DFT+ U theory [27] is employed where the DFT energy is captured by the Perdew-Burke-Ernzerhof (PBE)

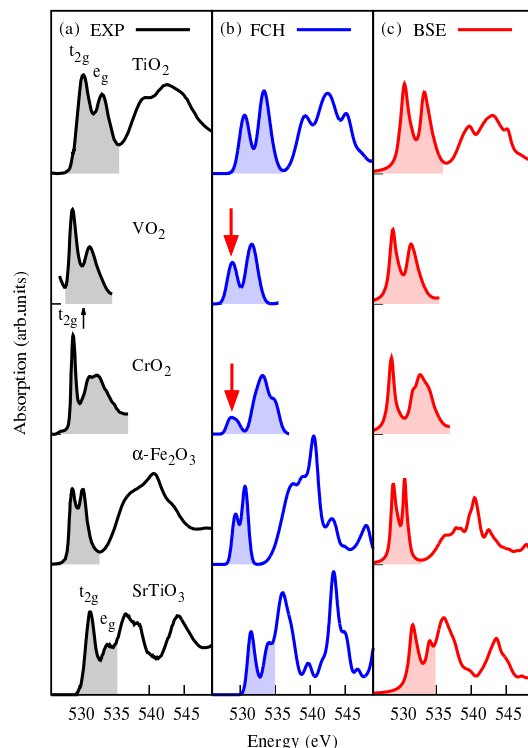


FIG. 1. A comparison of experimental O K edge (a) with the simulated spectra by the FCH approach (b) and BSE (c). The pre-edge regions are covered by shaded areas. Spectra are normalized according to the e_g peak intensity. The severely underestimated t_{2g} peaks are marked by red arrows.

functional, and the on-site Coulomb potential U are from Ref. [42]. We interpret the DFT+ U orbital energies as quasiparticle (QP) energies and perform FCH rather than XCH calculations so as not to favor any particular orbital. More numerical details can be found in the Supplemental Material [43].

Strikingly, the FCH approach systematically underestimates the near-edge peak associated with the t_{2g} manifold for all selected TMOs. The t_{2g} peak at 529.2 eV of CrO_2 [40] suffers from the most severe underestimation. It becomes a weak, broad feature in the FCH simulation as compared to the strong, sharp peak in experiment. The t_{2g} - e_g peak intensity ratios of VO_2 and Fe_2O_3 are also too low - both are predicted as 0.7, compared with 1.7 and 1.0 as measured, respectively. To validate the calculations, we have tested the numerical convergence with energy cutoffs and supercell sizes, and switched to local-density approximation functionals, but none of these suggests the failure of the FCH calculation is a numerical artifact or the impact of the empirical U values [43].

Bethe-Salpeter Equation Within the Tamm-Dancoff approximation (TDA) [33, 44, 45], the photo-excited state is a superposition of electron-hole (e - h) pairs

$$|\Phi_f\rangle = \sum_c A_c^f a_c^\dagger h^\dagger |\Phi_i\rangle \quad (3)$$

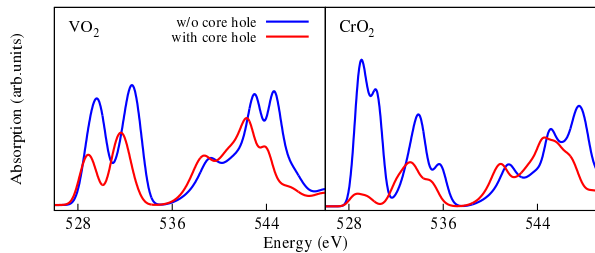


FIG. 2. A comparison of the spectra with and without (w/o) the core hole in the FCH calculations.

where a_c^\dagger and h^\dagger are the initial-state electron and the $1s$ core-hole creation operators respectively. The exciton amplitude A_c^f can be solved from the BSE

$$(\varepsilon_c - \varepsilon_h)A_c^f + \sum_{c'} K_{c,c'}^{eh} A_{c'}^f = E_f A_c^f \quad (4)$$

where $\varepsilon_{c,h}$ are single-particle energies of the initial-state orbitals. K^{eh} is the e - h interaction kernel, comprising a direct term $K^{eh,D}$ and an exchange term $K^{eh,X}$. E_f is the eigenenergy of the excitation. $K^{eh,D}$ involves the screened Coulomb interaction W obtained within the random phase approximation (RPA), whereas $K^{eh,X}$ involves the bare Coulomb interaction. The core-level BSE calculation is done with the OCEAN code [35, 46].

As is shown in Fig. 1 (c), the BSE substantially improves on the O K edge lineshape. The edge-sharpness of the lower-energy peak is retrieved for all the investigated TMOs, particularly for CrO_2 . The simulated t_{2g} - e_g intensity ratios are almost as measured for TiO_2 , $\alpha\text{-Fe}_2\text{O}_3$, and SrTiO_3 (below 537 eV). The BSE calculations systematically improve on the initial-state prediction of lineshape for the rutile group from previous studies [31, 47].

Discussion The core-hole effects in the O K edge as predicted by the ΔSCF method are counterintuitive. Typically, excitonic effects tend to sharpen the absorption edge due to e - h attraction [5, 32, 33, 44]. In Fig. 2 (b), we show the core-hole effects from FCH by comparing the initial- and final-state spectra. The core-hole attraction does redshift the spectra by more than 1 eV in both the pre-edge and $4sp$ [48] region (near 544 eV). However, the FCH core-hole effect substantially reduces the t_{2g} peak intensity. Similar underestimated pre-peak intensity was encountered before [49–51] but no satisfactory explanation has been provided to date.

The failure of the ΔSCF method in the pre-edge region motivates us to reexamine the approximations used in this approach as opposed to those in the BSE. The most obvious assumption that has been made is the approximation of the many-body matrix element in a single-body form. We now revisit the full many-body matrix element $\langle \Phi_f | \boldsymbol{\epsilon} \cdot \mathbf{R} | \Phi_i \rangle$. To this end, we express the final state $|\Phi_f\rangle$ in terms of the initial-state configurations. Since there is no restriction imposed on the initial configurations used in ΔSCF , its adiabatic final state goes beyond TDA-BSE

[Eq. (3)] and has incorporated the electronic response to the core-hole potential to all orders:

$$|\Phi_f\rangle = \left[\sum_c A_c^f a_c^\dagger h^\dagger + \sum_{c'cv} B_{c'cv}^f (a_c^\dagger b_v^\dagger) a_c^\dagger h^\dagger + \dots \right] |\Phi_i\rangle \quad (5)$$

where b_v^\dagger 's are valence-hole creation operators. $c(c')$ and v sum over all the *initial-state* empty and occupied orbitals respectively. However, despite the possible presence of one or more additional valence e - h pairs, such as $(a_c^\dagger b_v^\dagger) a_c^\dagger h^\dagger$, only the leading-order coefficient A_c^f can contribute to the many-body matrix element: $\langle \Phi_f | \boldsymbol{\epsilon} \cdot \mathbf{R} | \Phi_i \rangle = \sum_c (A_c^f)^* \langle \phi_c | \boldsymbol{\epsilon} \cdot \mathbf{r} | \phi_h \rangle$, because the dipole is a one-body operator. Thus it is sufficient to find A_c^f . This relies on a representation of the final state $|\Phi_f\rangle$ that has $N + 1$ valence electrons (the extra electron is the photoelectron). We extend the interpretation of the Kohn-Sham orbitals in the core hole approach and assume that a single Slater determinant of arbitrary $N + 1$ filled *final-state* Kohn-Sham orbitals is a good approximation of $|\Phi_f\rangle$, an eigenstate of the core-excited Hamiltonian. Now the final-state index f refers to a configuration of final-state orbitals $f = (f_1, f_2, \dots, f_{N+1})$ that the $N + 1$ electrons can occupy. Furthermore, the energy of $|\Phi_f\rangle$ (relative to the threshold energy E_{th}) is approximated as a non-interacting summation of the energies of all occupied final-state orbitals: $E_f = \sum_{\mu=1}^N \tilde{\varepsilon}_{f_\mu} - E_{\text{th}}$, where the threshold energy $E_{\text{th}} = \min_f E_f$, corresponds to the first final state configuration $(1, 2, \dots, N + 1)$. $|\Phi_f\rangle$ can be represented as

$$\begin{aligned} |\Phi_f\rangle &= \prod_{\mu=1}^{N+1} \tilde{\phi}_{f_\mu}^\dagger \prod_{\nu=1}^N b_\nu^\dagger h^\dagger |\Phi_i\rangle \\ &= \prod_{\mu=1}^{N+1} \left(\sum_c^{\text{empty}} \xi_{f_\mu,c} a_c^\dagger + \sum_v^{\text{occupied}} \xi_{f_\mu,v} b_v \right) \prod_{\nu=1}^N b_\nu^\dagger h^\dagger |\Phi_i\rangle \end{aligned} \quad (6)$$

in which all the $N + 1$ electrons are first removed via h^\dagger and $N b_\nu^\dagger$'s from the initial state, and then recreated via $N + 1 \tilde{\phi}_{f_\mu}^\dagger$'s to define the many-body final state. Note that a final-state orbital ϕ_f can in general be a hybridization of both the occupied (v) and empty (c) orbitals in the initial state due to the core-hole perturbation. ξ_{ij} 's are the transformation coefficients from the initial to final state [43]. As the core-hole effect on each initial-state orbital accumulates, $|\Phi_f\rangle$ in Eq. (6) reproduces the full many-electron response to the core-hole potential [Eq. (5)]. Ultimately, the expression for A_c^f can be obtained by combining the coefficients of the $a_c^\dagger h^\dagger$ term

$$A_c^f = \det \begin{bmatrix} \xi_{f_1,1} & \xi_{f_1,2} & \dots & \xi_{f_1,N} & \xi_{f_1,c} \\ \xi_{f_2,1} & \xi_{f_2,2} & \dots & \xi_{f_2,N} & \xi_{f_2,c} \\ \vdots & & \ddots & & \vdots \\ \xi_{f_{N+1},1} & \xi_{f_{N+1},2} & \dots & \xi_{f_{N+1},N} & \xi_{f_{N+1},c} \end{bmatrix} \quad (7)$$

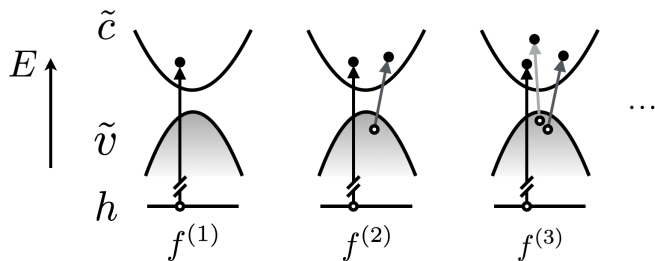


FIG. 3. Schematic of the excitation configurations in the final-state space. h indicates the single core level while \tilde{c} and \tilde{v} indicate the empty and occupied orbital spaces respectively.

Similar determinant expressions were also obtained in previous work [52–54] but they are rarely applied in a solid-state context from first-principles. Thus it is of great interest to examine whether the derived many-body Δ SCF formalism in Eq. (6) and (7) can reproduce the correct lineshapes for the investigated TMOs.

Evaluating A_c^f seems formidable at first glance because, unlike small molecules, a solid contains many electrons, which leads to huge number combinations of final states. To appreciate this, we regroup the final-state configurations according to the number of e - h pairs excited, by analogy to the initial-state decomposition in Eq. (5). For example, we denote a single configuration with one core-excited e - h pair as $f^{(1)} = (1, 2, \dots, N, f_{N+1})$, which is typically used in producing the one-body XAS in the core-hole approach and f_{N+1} is the orbital the photoelectron will occupy in the final state. Based on this configuration, we can define a double configuration with one more valence e - h pair as $f^{(2)} = (1, \dots, i-1, i+1, \dots, N, f_N, f_{N+1})$, where $f_{N+1} > f_N > N$, and so forth (Fig. 3). Despite a large number of excitation configurations, not all of them contribute equally to the XANES absorbance. First, for an insulator, the energy Ω_f of the final states will increase rapidly with the number of e - h pairs excited across the band gap (E_g): $E_f \geq (n-1)E_g$. This largely reduces the number of necessary final-states for producing the first few eVs of XANES for an insulator. Second, the many-body overlap may decrease rapidly with increasing number of e - h pairs excited, as we will show next.

Fig. 4 shows the XAS calculated from the many-body matrix element as in Eq. (6) and (7). The wavefunctions and the overlap matrix elements ξ_{ij} used for A_c^f are obtained from exactly the same set of FCH calculations [43] as previously described. For simplicity, only the states at the Γ -point of the supercell Brillouin zone are used for producing the XAS. We reexamine two extreme cases: the insulating TiO_2 and the metallic CrO_2 . Remarkably, the simulated XAS lineshapes with the many-body correction are in excellent agreement with experiments. In particular for CrO_2 , the edge sharpness is completely retrieved despite the disappearance of the first peak in a

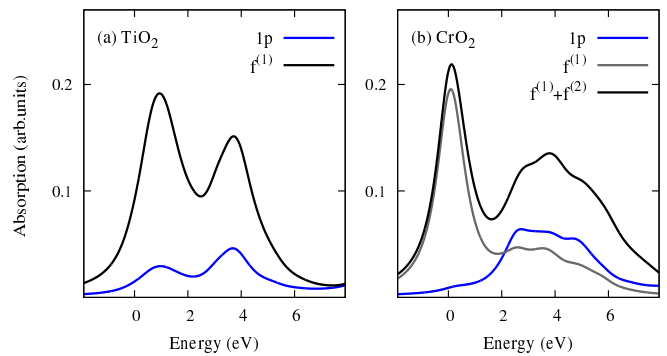


FIG. 4. Δ SCF XAS rectified by the many-body matrix formalism for TiO_2 (a) and CrO_2 (b). For comparison, the spectra produced by the one-body FCH formalism are denoted as 1p FCH. The absorption threshold is aligned at $E = 0$.

single-body theory.

When calculating the XAS for TiO_2 , we find its spectrum already converges at the order of $f^{(1)}$. As expected, the contributions from $f^{(2)}$ are at higher energies due to the sizable band gap, and are much weaker due to reduced many-body overlap. However, it is harder to achieve convergence in the metallic CrO_2 . While the first peak is retrieved mainly from low-order excitations $f^{(1)}$, the correct peak-intensity ratio can only be reproduced when the next-order $f^{(2)}$ is taken into account, which substantially intensifies the absorption feature, ~ 4 eV above onset. We find $f^{(3)}$ can be neglected up to the first 8 eV.

At last, we explain why the one-body Δ SCF formalism tends to underestimate the peak intensity. With S constant, Eq. (2) produces nothing but an RPA absorption spectrum in the final-state picture in which the charge density has equilibrated with the core-hole potential. No charge relaxation dynamics are involved. In the this adiabatic final state of O $1s$ excitations, a substantial amount of electron density is transferred onto the $2p$ state of the excited O ($0.55 e^-$ for TiO_2 and $0.72 e^-$ for CrO_2), which eventually blocks some bright transitions from $1s \rightarrow 2p$ and leads to the reduced pre-edge intensity. On the other hand, both BSE and the many-body Δ SCF formalism have taken into account the excitation dynamics from the initial state to the final state. In both the BSE [Eq. (3)] and the many-body formalism [Eq. (6)], only the initial empty states ϕ_c are involved and thus the edge sharpness is captured.

Conclusions We have shown that the BSE and a newly developed many-body Δ SCF approach are highly predictive for O K -edge fingerprints of TMOs. The systematic underestimation of the peak-intensity ratio within the original one-body Δ SCF approach is attributed to the absence of many-electron excitation dynamics in this formalism. We have demonstrated how to rectify these shortcomings (1) an expansion of the final-state configurations in terms of Slater determinants; (2)

a projection of these final states onto the initial-state orbital basis; and (3) a correct accounting of the relevant component of the adiabatic final state accessible to dipole transitions. This many-body formalism is transferable and not at all not peculiar to TMOs. In fact, the expansion in Eq. (6) goes beyond the BSE formalism and is more universal. We leave the discussion of shakeup effects, improvement of efficiency, and other examples to near-future work.

Acknowledgement Theoretical and computational work was performed by Y. L. and D. P. at The Molecular Foundry, which is supported by the Office of Science, Office of Basic Energy Sciences, of the United States Department of Energy under Contact No. DE-AC02-05CH11231. We acknowledge fruitful discussion with Chunjing Jia (Y. L.) and Bill Gadzuk (J. V.). Computations were performed with the computing resources at the National Energy Research Scientific Computing Center (NERSC).

* yufengliang@lbl.gov

- [1] Janel S Uejio, Craig P Schwartz, Richard J Saykally, and David Prendergast. Effects of vibrational motion on core-level spectra of prototype organic molecules. *Chemical Physics Letters*, 467(1):195–199, 2008.
- [2] L Triguero, LGM Pettersson, and H Ågren. Calculations of near-edge x-ray-absorption spectra of gas-phase and chemisorbed molecules by means of density-functional and transition-potential theory. *Physical Review B*, 58(12):8097, 1998.
- [3] Teruyasu Mizoguchi, Isao Tanaka, Masato Yoshiya, Fumiyasu Oba, Kazuyoshi Ogasawara, and Hirohiko Adachi. Core-hole effects on theoretical electron-energy-loss near-edge structure and near-edge x-ray absorption fine structure of mgo. *Physical Review B*, 61(3):2180, 2000.
- [4] Shang-Di Mo and WY Ching. Ab initio calculation of the core-hole effect in the electron energy-loss near-edge structure. *Physical Review B*, 62(12):7901, 2000.
- [5] G Duscher, R Buczko, SJ Pennycook, and SI T Pantelides. Core-hole effects on energy-loss near-edge structure. *Ultramicroscopy*, 86(3):355–362, 2001.
- [6] Mathieu Taillefumier, Delphine Cabaret, Anne-Marie Flank, and Francesco Mauri. X-ray absorption near-edge structure calculations with the pseudopotentials: Application to the k edge in diamond and α -quartz. *Physical Review B*, 66(19):195107, 2002.
- [7] Balázs Hetényi, Filippo De Angelis, Paolo Giannozzi, and Roberto Car. Calculation of near-edge x-ray-absorption fine structure at finite temperatures: Spectral signatures of hydrogen bond breaking in liquid water. *The Journal of chemical physics*, 120(18):8632–8637, 2004.
- [8] Matteo Cavalleri, Michael Odelius, Dennis Nordlund, Anders Nilsson, and Lars GM Pettersson. Half or full core hole in density functional theory x-ray absorption spectrum calculations of water? *Physical Chemistry Chemical Physics*, 7(15):2854–2858, 2005.
- [9] David Prendergast and Giulia Galli. X-ray absorption spectra of water from first principles calculations. *Physical Review Letters*, 96(21):215502, 2006.
- [10] Juan-Jesus Velasco-Velez, Cheng Hao Wu, Tod A Pascal, Liwen F Wan, Jinghua Guo, David Prendergast, and Miquel Salmeron. The structure of interfacial water on gold electrodes studied by x-ray absorption spectroscopy. *Science*, 346(6211):831–834, 2014.
- [11] Naoaki Yabuuchi, Kazuhiro Yoshii, Seung-Taek Myung, Izumi Nakai, and Shinichi Komaba. Detailed studies of a high-capacity electrode material for rechargeable batteries, $\text{Li}_2\text{MnO}_3\text{-LiCo}_1/3\text{Ni}_1/3\text{Mn}_1/3\text{O}_2$. *Journal of the American Chemical Society*, 133(12):4404–4419, 2011.
- [12] Yan-Yan Hu, Zigeng Liu, Kyung-Wan Nam, Olaf J Borkiewicz, Jun Cheng, Xiao Hua, Matthew T Dunstan, Xiqian Yu, Kamila M Wiaderek, Lin-Shu Du, et al. Origin of additional capacities in metal oxide lithium-ion battery electrodes. *Nature materials*, 12(12):1130–1136, 2013.
- [13] Feng Lin, Dennis Nordlund, Yuyi Li, Matthew K Quan, Lei Cheng, Tsu-Chien Weng, Yijin Liu, Huolin L Xin, and Marca M Doeff. Metal segregation in hierarchically structured cathode materials for high-energy lithium batteries. *Nature Energy*, 1:15004, 2016.
- [14] Kun Luo, Matthew R Roberts, Rong Hao, Niccoló Guerini, David M Pickup, Yi-Sheng Liu, Kristina Edström, Jinghua Guo, Alan V Chadwick, Laurent C Duda, et al. Charge-compensation in 3d-transition-metal-oxide intercalation cathodes through the generation of localized electron holes on oxygen. *Nature Chemistry*, 2016.
- [15] Jin Suntivich, Hubert A Gasteiger, Naoaki Yabuuchi, Haruyuki Nakanishi, John B Goodenough, and Yang Shao-Horn. Design principles for oxygen-reduction activity on perovskite oxide catalysts for fuel cells and metal-air batteries. *Nature chemistry*, 3(7):546–550, 2011.
- [16] Peter Strasser, Shirlaine Koh, Toyli Anniyev, Jeff Greeley, Karren More, Chengfei Yu, Zengcai Liu, Sarp Kaya, Dennis Nordlund, Hirohito Ogasawara, et al. Lattice-strain control of the activity in dealloyed core-shell fuel cell catalysts. *Nature chemistry*, 2(6):454–460, 2010.
- [17] Guo-zhen Zhu, Guillaume Radtke, and Gianluigi A Botton. Bonding and structure of a reconstructed (001) surface of SrTiO_3 from tem. *Nature*, 490(7420):384–387, 2012.
- [18] Michinori Matsukawa, Ryo Ishikawa, Takashi Hisatomi, Yosuke Moriya, Naoya Shibata, Jun Kubota, Yuichi Ikuhara, and Kazunari Domen. Enhancing photocatalytic activity of LaTiO_2N by removal of surface reconstruction layer. *Nano letters*, 14(2):1038–1041, 2014.
- [19] Alexis Grimaud, Kevin J May, Christopher E Carlton, Yueh-Lin Lee, Marcel Risch, Wesley T Hong, Jigang Zhou, and Yang Shao-Horn. Double perovskites as a family of highly active catalysts for oxygen evolution in alkaline solution. *Nature communications*, 4, 2013.
- [20] Z Lebens-Higgins, DO Scanlon, H Paik, S Sallis, Y Nie, M Uchida, NF Quackenbush, MJ Wahila, GE Sterbinsky, Dario A Arena, et al. Direct observation of electrostatically driven band gap renormalization in a degenerate perovskite transparent conducting oxide. *Phys Rev Lett*, 116:027602, 2016.
- [21] TC Koethe, Z Hu, MW Haverkort, C Schüßler-Langeheine, F Venturini, NB Brookes, Oscar Tjernberg, W Reichelt, HH Hsieh, H-J Lin, et al. Transfer of spectral weight and symmetry across the metal-insulator transition in VO_2 . *Physical review letters*, 97(11):116402, 2006.

- [22] Dmitry Ruzmetov, Sanjaya D Senanayake, and Shriram Ramanathan. X-ray absorption spectroscopy of vanadium dioxide thin films across the phase-transition boundary. *Physical Review B*, 75(19):195102, 2007.
- [23] Nagaphani B Aetukuri, Alexander X Gray, Marc Drouard, Matteo Cossale, Li Gao, Alexander H Reid, Roopali Kukreja, Hendrik Ohldag, Catherine A Jenkins, Elke Arenholz, et al. Control of the metal-insulator transition in vanadium dioxide by modifying orbital occupancy. *Nature Physics*, 9(10):661–666, 2013.
- [24] CT Chen, F Sette, Y Ma, MS Hybertsen, EB Stechel, WMC Foulkes, M Schuller, SW Cheong, AS Cooper, LW Rupp Jr, et al. Electronic states in $\text{La}_2\text{-xSr}_x\text{CuO}_{4+\delta}$ probed by soft-x-ray absorption. *Physical review letters*, 66(1):104, 1991.
- [25] DC Peets, DG Hawthorn, KM Shen, Young-June Kim, DS Ellis, H Zhang, Seiki Komiya, Yoichi Ando, GA Sawatzky, Ruixing Liang, et al. X-ray absorption spectra reveal the inapplicability of the single-band hubbard model to overdoped cuprate superconductors. *Physical review letters*, 103(8):087402, 2009.
- [26] J-S Lee, YW Xie, HK Sato, C Bell, Y Hikita, HY Hwang, and C-C Kao. Titanium dxy ferromagnetism at the $\text{LaO}_3/\text{SrTiO}_3$ interface. *Nature materials*, 12(8):703–706, 2013.
- [27] SL Dudarev, GA Botton, SY Savrasov, CJ Humphreys, and AP Sutton. Electron-energy-loss spectra and the structural stability of nickel oxide: An LSDA+U study. *Physical Review B*, 57(3):1505, 1998.
- [28] VI Anisimov, Dm M Korotin, MA Korotin, AV Kozhevnikov, J Kuneš, AO Shorikov, SL Skornyakov, and SV Streltsov. Coulomb repulsion and correlation strength in LaFeO_3 from density functional and dynamical mean-field theories. *Journal of Physics: Condensed Matter*, 21(7):075602, 2009.
- [29] Xin Wang, Luca de Medici, and AJ Millis. Theory of oxygen k edge x-ray absorption spectra of cuprates. *Physical Review B*, 81(9):094522, 2010.
- [30] C-C Chen, M Sentef, YF Kung, CJ Jia, R Thomale, B Moritz, AP Kampf, and TP Devereaux. Doping evolution of the oxygen k-edge x-ray absorption spectra of cuprate superconductors using a three-orbital hubbard model. *Physical Review B*, 87(16):165144, 2013.
- [31] Frank De Groot and Akio Kotani. *Core level spectroscopy of solids*. CRC press, 2008.
- [32] Eric L Shirley. Ab initio inclusion of electron-hole attraction: Application to x-ray absorption and resonant inelastic x-ray scattering. *Physical Review Letters*, 80(4):794, 1998.
- [33] Lorin X Benedict, Eric L Shirley, and Robert B Bohn. Optical absorption of insulators and the electron-hole interaction: An ab initio calculation. *Physical review letters*, 80(20):4514, 1998.
- [34] JJ Rehr, JA Soininen, and EL Shirley. Final-state rule vs the bethe-salpeter equation for deep-core x-ray absorption spectra. *Physica Scripta*, 2005(T115):207, 2005.
- [35] J Vinson, JJ Rehr, JJ Kas, and EL Shirley. Bethe-salpeter equation calculations of core excitation spectra. *Physical Review B*, 83(11):115106, 2011.
- [36] Tod A Pascal, Kevin H Wujcik, Juan Velasco-Velez, Chenghao Wu, Alexander A Teran, Mukes Kapilashrami, Jordi Cabana, Jinghua Guo, Miquel Salmeron, Nitash Balsara, et al. X-ray absorption spectra of dissolved polysulfides in lithium-sulfur batteries from first-principles. *The journal of physical chemistry letters*, 5(9):1547–1551, 2014.
- [37] Thomas M McDonald, Jarad A Mason, Xueqian Kong, Eric D Bloch, David Gygi, Alessandro Dani, Valentina Crocellà, Filippo Giordanino, Samuel O Odoh, Walter S Drisdell, et al. Cooperative insertion of CO_2 in diamine-appended metal-organic frameworks. *Nature*, 519(7543):303–308, 2015.
- [38] Tod A Pascal, Ulrike Boesenberg, Robert Kostecki, Thomas J Richardson, Tsu-Chien Weng, Dimosthenis Sokaras, Dennis Nordlund, Eamon McDermott, Alexander Moewes, Jordi Cabana, et al. Finite temperature effects on the x-ray absorption spectra of lithium compounds: First-principles interpretation of x-ray raman measurements. *The Journal of chemical physics*, 140(3):034107, 2014.
- [39] Wensheng Yan, Zhihu Sun, Zhiyun Pan, Qinghua Liu, Tao Yao, Ziyu Wu, Cheng Song, Fei Zeng, Yaning Xie, Tiandou Hu, et al. Oxygen vacancy effect on room-temperature ferromagnetism of rutile CoTiO_3 thin films. *Applied Physics Letters*, 94(4):42508, 2009.
- [40] CB Stagaescu, X Su, DE Eastman, KN Altmann, FJ Himpsel, and A Gupta. Orbital character of $\text{O} 2p$ unoccupied states near the fermi level in CuO . *Physical Review B*, 61(14):R9233, 2000.
- [41] Shaohua Shen, Jigang Zhou, Chung-Li Dong, Yongfeng Hu, Eric Nestor Tseng, Penghui Guo, Liejin Guo, and Samuel S Mao. Surface engineered doping of hematite nanorod arrays for improved photoelectrochemical water splitting. *Scientific reports*, 4, 2014.
- [42] Lei Wang, Thomas Maxisch, and Gerbrand Ceder. Oxidation energies of transition metal oxides within the $\text{GGA}+U$ framework. *Physical Review B*, 73(19):195107, 2006.
- [43] Supplemental materials.
- [44] Michael Rohlfing and Steven G Louie. Electron-hole excitations and optical spectra from first principles. *Physical Review B*, 62(8):4927, 2000.
- [45] Giovanni Onida, Lucia Reining, and Angel Rubio. Electronic excitations: density-functional versus many-body green's-function approaches. *Reviews of Modern Physics*, 74(2):601, 2002.
- [46] K Gilmore, John Vinson, EL Shirley, D Prendergast, CD Pemmaraju, JJ Kas, FD Vila, and JJ Rehr. Efficient implementation of core-excitation bethe-salpeter equation calculations. *Computer Physics Communications*, 197:109–117, 2015.
- [47] Frank De Groot. High-resolution x-ray emission and x-ray absorption spectroscopy. *Chemical Reviews*, 101(6):1779–1808, 2001.
- [48] FMF De Groot, M Grioni, JC Fuggle, J Ghijsen, GA Sawatzky, and H Petersen. Oxygen $1s$ x-ray-absorption edges of transition-metal oxides. *Physical Review B*, 40(8):5715, 1989.
- [49] Amélie Juhin, Frank De Groot, György Vankó, Matteo Calandra, and Christian Broder. Angular dependence of core hole screening in LiCoO_2 : A $\text{dft}+U$ calculation of the oxygen and cobalt k-edge x-ray absorption spectra. *Physical Review B*, 81(11):115115, 2010.
- [50] Isao Tanaka, Teruyasu Mizoguchi, and Tomoyuki Yamamoto. Xanes and elnes in ceramic science. *Journal of the American Ceramic Society*, 88(8):2013–2029, 2005.
- [51] V Kanchana, G Vaitheeswaran, and M Alouani. Calculated electronic structure and x-ray magnetic circular dichroism of CuO . *Journal of Physics: Condensed Mat-*

- ter, 18(22):5155, 2006.
- [52] PHILIP W Anderson. Infrared catastrophe in fermi gases with local scattering potentials. *Physical Review Letters*, 18(24):1049, 1967.
- [53] Edward A Stern and John J Rehr. Many-body aspects of the near-edge structure in x-ray absorption. *Physical Review B*, 27(6):3351, 1983.
- [54] K Ohtaka and Y Tanabe. Theory of the soft-x-ray edge problem in simple metals: historical survey and recent developments. *Reviews of Modern Physics*, 62(4):929, 1990.